

## AN INVESTIGATION OF STOKES' SECOND PROBLEM FOR NON-NEWTONIAN FLUIDS

L. Ai and K. Vafai

*Department of Mechanical Engineering, University of California at Riverside, Riverside, California, USA*

*Stokes flow produced by an oscillatory motion of a wall is analyzed in the presence of a non-Newtonian fluid. A total of eight non-Newtonian models are considered. A mass balance approach is introduced to solve the governing equations. The velocity and temperature profiles for these models are obtained and compared to those of Newtonian fluids. For the power law model, correlations for the velocity distribution and the time required to reach the steady periodic flow are developed and discussed. Furthermore, the effects of the dimensionless parameters on the flow are studied. For the temperature distribution, an analytical solution for Newtonian fluid is developed as a comparative source. To simulate the rheological behavior of blood at unsteady state, three non-Newtonian constitutive relationships are used to study the wall shear stress. It is found that in the case of unsteady Stokes flow, although the patterns of velocity and wall shear stress is consistent across all models, the magnitude is affected by the model utilized.*

### 1. INTRODUCTION

Stokes' first problem refers to the shear flow of a viscous fluid near a flat plate which is suddenly accelerated from rest and moves in its own plane with a constant velocity. If the flat plate executes linear harmonic oscillations parallel to itself, the problem is referred to as Stokes' second problem [1]. It admits an analytical solution. The study of Stokes' second problem has some applications in the fields of chemical, medical, biomedical, micro, and nanotechnology. An illustrative example is the shear-driven pump in microfluidic devices. The solution of the Stokes' problem under vibrating wall condition that satisfies the no-slip condition at the wall has been studied in depth by Erdogan [2]. Recently, exact solutions including both steady periodic and transient velocity profiles for Stokes' and Couette flows subject to slip conditions were given in the work of Khaled and Vafai [3]. In the work of Johnston et al. [4], five non-Newtonian models for blood flow at steady state were studied. However, the literature lacks studies that take into account the presence of non-Newtonian fluids for Stokes' second problem.

Among the non-Newtonian models, the second-grade model is able to predict the normal stress differences which are characteristic of non-Newtonian fluids. However, the shear viscosity is constant in the second-grade model. As such, a

Received 15 September 2004; accepted 24 November 2004.

Address correspondence to K. Vafai, Department of Mechanical Engineering, A363 Bourns Hall, University of California at Riverside, Riverside, CA 92521-0425, USA. E-mail: vafai@engr.ucr.edu

### NOMENCLATURE

$c_p$	heat capacity	$\dot{\gamma}$	generalized shear rate
$Ek$	Eckert number	$\dot{\gamma}_0$	reference shear rate
$f$	harmonic averaged function	$\eta$	dimensionless normal coordinate
$h$	grid spacing	$\theta$	dimensionless temperature
$k$	time step	$\kappa$	dimensionless parameter
$k_f$	thermal conductivity	$\lambda$	characteristic time
$K$	consistency coefficient	$\mu$	dynamic viscosity of the fluid
$n$	power-law index	$\mu_0$	zero-shear viscosity
$Pr$	Prandtl number	$\mu_\infty$	viscosity at very high shear rates
$q$	flux	$\nu$	kinematic viscosity
$t$	time	$\nu_0$	representative viscosity of the Newtonian fluid
$T_0$	temperature of the plate	$\rho$	density
$u_w$	velocity of the plate	$\tau$	dimensionless time
$U, u$	dimensionless and dimensional velocities	$\Phi$	dissipation function
$U_0$	reference velocity	$\omega$	frequency of the vibration
$y$	dimensional normal coordinate		

shear-thinning or shear-thickening fluid cannot be predicted by a second-grade model. The third-grade model exhibits shear-dependent viscosity. Examples can be found in chemical engineering, where in some industrial processes, steady and unsteady shear flows with non-Newtonian behavior are involved. In this work, the non-Newtonian behavior for the Stokes second problem is investigated. As the shear-dependent viscosity models are introduced, the governing equations become nonlinear. The solutions are obtained by using a mass balance argument to obtain a discrete version of the governing equation. The mass balance approach [5] yields a system of difference equations that ensures the conservation of mass.

## 2. BASIC EQUATIONS

The schematic of the problem under consideration is shown in Figure 1. The  $x$  coordinate is parallel to the plate and the fluid occupies the space  $y > 0$ , with the  $y$  axis in the vertical direction. The plate is initially at rest. At time  $t = 0^+$ , the plate is subjected to a velocity  $u_w = U_0 \cos \omega t$  in its own plane, resulting in the induced flow. The governing momentum equation is

$$\rho \frac{\partial u}{\partial t} = \frac{\partial}{\partial y} \left( \mu \frac{\partial u}{\partial y} \right) \quad (1)$$

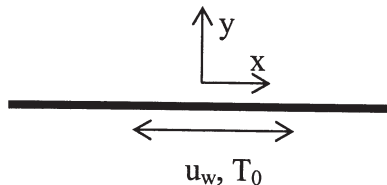


**Figure 1.** Schematic diagram of Stokes' second problem.

where  $u$ ,  $t$ , and  $\mu$  are the velocity in the  $x$  direction, time, and the dynamic viscosity of the fluid, respectively. For the problem under consideration, the initial condition is

$$u(y, 0) = 0 \quad (2)$$

and the boundary conditions considered in this work are given by

$$\begin{aligned} u(y, t) &= U_0 \cos \omega t & \text{at } y = 0 \text{ for } t > 0 \\ u(\infty, t) &= 0 \end{aligned} \quad (3a)$$

where  $U_0$  is the representative velocity and  $\omega$  is the frequency of the oscillation at the wall.

Another set of boundary conditions is

$$\begin{aligned} u(y, t) &= U_0 \sin \omega t & \text{at } y = 0 \text{ for } t > 0 \\ u(\infty, t) &= 0 \end{aligned} \quad (3b)$$

The energy equation for the case under consideration can be written as

$$\rho c_p \frac{\partial T}{\partial t} = \frac{\partial}{\partial y} \left( k_f \frac{\partial T}{\partial y} \right) + \mu \Phi \quad (4)$$

where  $\Phi = (\partial u / \partial y)^2$  represents the dissipation function and  $k_f$  represents the conductivity of the fluid. The initial and boundary conditions are

$$\begin{aligned} T(y, 0) &= T_\infty \\ T(y, t) &= T_0 & \text{at } y = 0 \text{ for } t > 0 \\ T_y(\infty, t) &= 0 \end{aligned} \quad (5)$$

### 3. NON-NEWTONIAN FLUID MODELS

It is well known that some fluids which are encountered in chemical applications do not adhere to the classical Newtonian viscosity prescription and are accordingly known as non-Newtonian fluids. One especial class of fluids which are of considerable practical importance is that in which the viscosity depends on the shear stress or on the flow rate. The viscosity of most non-Newtonian fluids, such as polymers, is usually a nonlinear decreasing function of the generalized shear rate  $\dot{\gamma}$ . This is known as shear-thinning behavior. The most commonly used expression for the viscosity is the power-law or Ostwald-de-Waele model [6, 7]:

$$\mu(\dot{\gamma}) = K |\dot{\gamma}|^{n-1} \quad (6)$$

where  $K$  is called the consistency coefficient and  $n$  is the power-law index. The index  $n$  is nondimensional, and the dimension of  $K$  depends on the value of  $n$ . The parameter  $n$  is an important index to subdivide fluids into pseudo-plastic fluids (when  $n < 1$ ) and dilatant fluids (when  $n > 1$ ). The two extreme cases of the power-law model are  $n = 1$  for Newtonian behavior and  $n = 0$  for plastic or solid behavior.

A major drawback of the power-law model is that it predicts an infinite viscosity (when  $n < 1$ ) as the shear rate tends to zero. However, the actual viscosity of molten polymers has a finite and constant value at very low shear rates.

Another commonly used non-Newtonian model based on molecular considerations [8] is referred to as the Prandtl-Eyring model:

$$\mu(\dot{\gamma}) = \mu_0 \frac{\sinh^{-1}(\lambda\dot{\gamma})}{\lambda\dot{\gamma}} \quad (7)$$

where  $\mu_0$  is the zero-shear viscosity. It has the dimensions of the viscosity and is indeed equal to the lower limiting viscosity, i.e.,  $\dot{\gamma} \rightarrow 0, \mu \rightarrow \mu_0$ , and the parameter  $\lambda$  is a characteristic time. This model predicts pseudo-plastic behavior, but it fails to predict an upper limiting viscosity.

The drawback of the Prandtl-Eyring model is eliminated by a slightly more complicated form of the  $\mu(\dot{\gamma})$  function, usually referred to as the Powell-Eyring model [8] and given by

$$\mu(\dot{\gamma}) = \mu_\infty + (\mu_0 - \mu_\infty) \frac{\sinh^{-1}(\lambda\dot{\gamma})}{\lambda\dot{\gamma}} \quad (8)$$

where  $\mu_\infty$  is a constant viscosity at very high shear rates.

Another non-Newtonian model considered here is the hyperbolic tangent model [7]:

$$\mu(\dot{\gamma}) = \mu_\infty + (\mu_0 - \mu_\infty) \tanh(\lambda\dot{\gamma})^n \quad (9)$$

The viscous properties of an emulsion are best described by the Sisko and Carreau models. The Sisko model [9] is given by

$$\mu(\dot{\gamma}) = \mu_0 + K\dot{\gamma}^{n-1} \quad (10)$$

where the parameters  $\mu_0, \mu_\infty, \lambda,$  and  $n$  are obtained from experimental data. The Carreau model [7] is described by

$$\mu(\dot{\gamma}) = \mu_\infty + \frac{\mu_0 - \mu_\infty}{[1 + (\lambda\dot{\gamma})^2]^{(1-n)/2}} \quad (11)$$

Among these models, the Powell-Eyring model, the Carreau model, and the hyperbolic tangent model verify the two Newtonian limits:

$$\mu = \begin{cases} \mu_0 & \dot{\gamma} \rightarrow 0 \\ \mu_\infty & \dot{\gamma} \rightarrow \infty \end{cases} \quad (12)$$

To simulate the rheological behavior of blood at unsteady state, three non-Newtonian constitutive relationships have been employed here [10].

**Power-Law Model**

$$\mu(\dot{\gamma}) = K|\dot{\gamma}|^{n-1} \tag{13}$$

**Casson Model**

The Casson model was first proposed by Casson [11] for shear-thinning fluids, such as printer ink. It has the following stress–strain rate relationship:

$$\sqrt{\tau} = \sqrt{\mu_\infty \dot{\gamma}} + \sqrt{\tau_y} \tag{14}$$

where  $\tau_y$  is the yield stress and  $\mu_\infty$  is called Casson viscosity or the asymptotic viscosity. The Casson model is valid for a wide range of shear rates, from  $1 \text{ s}^{-1}$  to  $100,000 \text{ s}^{-1}$ , according to the work of Charm and Kurland [12]. However, it is difficult to apply Casson’s equation in numerical schemes due to its discontinuous character. Accordingly, the weak Casson model as given by Papanastasiou [13] is usually utilized:

$$\mu(\dot{\gamma}) = \left[ \sqrt{\mu_\infty} + \sqrt{\frac{\tau_y}{\dot{\gamma}}} \left( 1 - e^{-\sqrt{m|\dot{\gamma}|}} \right) \right]^2 \tag{15}$$

which has been found [14] to approach Casson’s equation for  $m > 100$ .

**Quemada Model**

The Quemada model was proposed by Quemada [15] to predict the viscosity of concentrated disperse systems, based on shear rate and hematocrit.

$$\mu(\dot{\gamma}) = \mu_0 \left( 1 - \frac{1}{2} \frac{k_0 + k_\infty \sqrt{\dot{\gamma}/\dot{\gamma}_c}}{1 + \sqrt{\dot{\gamma}/\dot{\gamma}_c}} \phi \right)^{-2} \tag{16}$$

where  $\mu_0$  is the viscosity of plasma (suspending medium) and  $\phi$  is the hematocrit.

According to several studies [12, 15–17], typical values for the coefficients in Eqs. (13), (15), and (16) are listed in Table 1.

**4. NONDIMENSIONAL FORMULATION**

For the governing equations, we introduce the nondimensional quantities defined by

$$U = \frac{u}{U_0} \quad \tau = \omega t \quad \eta = y \left( \frac{\omega}{\nu_0} \right)^{1/2} \quad \theta = \frac{T - T_\infty}{T_0 - T_\infty} \tag{17}$$

**Table 1** Rheology model constants

Power law	$K = 14.67 \times 10^{-3} \text{ Pa s}^n, n = 0.7755$
Casson	$\tau_y = 10.82 \text{ mPa}, \mu_\infty = 3.1 \times 10^{-3} \text{ Pa s}, m = 100 \text{ s}$
Quemada	$\mu_0 = 1.2 \times 10^{-3} \text{ Pa s}, \phi = 0.45, \dot{\gamma}_c = 1.88 \text{ s}^{-1}, k_0 = 4.33, k_\infty = 2.07$

Hence, we have

$$\frac{\partial u}{\partial y} = U_0 \frac{\partial U}{\partial \eta} \frac{\partial \eta}{\partial y} = U_0 \left( \frac{\omega}{\nu_0} \right)^{1/2} \frac{\partial U}{\partial \eta}$$

$$\frac{\partial u}{\partial t} = U_0 \frac{\partial U}{\partial \tau} \frac{\partial \tau}{\partial t} = U_0 \omega \frac{\partial U}{\partial \tau}$$

where  $\nu_0$  is the reference viscosity of the Newtonian fluid. Therefore the nondimensional form of the momentum equation can be written as

$$\frac{\partial U}{\partial \tau} = \frac{\partial}{\partial \eta} \left[ \frac{\mu(U_\eta)}{\mu_0} \frac{\partial U}{\partial \eta} \right] \quad (18)$$

For example, the nondimensional momentum equation for the power-law model will be

$$\frac{\partial U}{\partial \tau} = \kappa \frac{\partial}{\partial \eta} \left( \left| \frac{\partial U}{\partial \eta} \right|^{n-1} \frac{\partial U}{\partial \eta} \right) \quad (19)$$

where  $\kappa = (K/\mu_0) U_0^{n-1} (\omega/\nu_0)^{(n-1)/2}$ .

The boundary conditions are

$$U(\eta, 0) = 0 \quad U(0, \tau) = \sin \tau \text{ or } \cos \tau \quad U(\infty, \tau) = 0 \quad (20)$$

For the energy equation, we have

$$\frac{\partial T}{\partial y} = (T_0 - T_\infty) \frac{\partial \theta}{\partial \eta} \frac{\partial \eta}{\partial y} = (T_0 - T_\infty) \left( \frac{\omega}{\nu_0} \right)^{1/2} \frac{\partial \theta}{\partial \eta}$$

$$\frac{\partial^2 T}{\partial y^2} = (T_0 - T_\infty) \left( \frac{\omega}{\nu_0} \right)^{1/2} \frac{\partial^2 \theta}{\partial \eta^2} \frac{\partial \eta}{\partial y} = (T_0 - T_\infty) \left( \frac{\omega}{\nu_0} \right) \frac{\partial^2 \theta}{\partial \eta^2}$$

$$\frac{\partial T}{\partial t} = (T_0 - T_\infty) \frac{\partial \theta}{\partial \tau} \frac{\partial \tau}{\partial t} = (T_0 - T_\infty) \omega \frac{\partial \theta}{\partial \tau}$$

Hence, the nondimensional energy equation can be written as

$$\frac{\partial \theta}{\partial \tau} = \frac{1}{\text{Pr}} \frac{\partial^2 \theta}{\partial \eta^2} + \text{Ek} \frac{\mu(U_\eta)}{\mu_0} \left( \frac{\partial U}{\partial \eta} \right)^2 \quad (21)$$

where Pr is the Prandtl number, Ek is the Eckert number,  $\mu_0$  is the dynamic viscosity of the Newtonian fluid, and  $\mu(U_\eta)$  is the viscosity of the non-Newtonian fluid. The expression for  $\mu(U_\eta)$  depends on the viscosity model applied. For example, the nondimensional energy equation for the power-law model will be

$$\frac{\partial \theta}{\partial \tau} = \frac{1}{\text{Pr}} \frac{\partial^2 \theta}{\partial \eta^2} + \kappa \text{Ek} \left| \frac{\partial U}{\partial \eta} \right|^{n+1} \quad (22)$$

where  $\kappa = (K/\mu_0)U_0^{n-1}(\omega/\nu_0)^{(n-1)/2}$ . And the temperature boundary and initial conditions can be written as

$$\theta(0, \tau) = 1 \quad \theta_\eta(\infty, \tau) = 0 \quad \theta(\eta, 0) = 0 \tag{23}$$

### 5. NUMERICAL SIMULATION

An effective finite-difference procedure is developed to solve the nonlinear equations. A material balance argument is utilized to obtain the discrete version of the nonlinear momentum equation. To illustrate a material balance approach in developing difference equations, we use the following notation to simplify the nondimensional version of the momentum equation:

$$s(u)u_t - [a(u)u_x]_x = 0 \tag{24}$$

Equation (24) represents a conservation law in the sense that a density  $\rho$  and a flux  $q$  can be related to  $u$  with equations of the form  $\rho_t = s(u)u_t$  and  $q = -a(u)u_x$ , so that that Eq. (24) is equivalent to the balance equation

$$\rho_t + q_x = 0 \tag{25}$$

For the uniform  $x$ -grid distribution as shown in Figure 2,  $x_n = nh$ ,  $n = 0, 1, 2, \dots, N + 1$ . Also define a set of points on the  $x$  axis by  $\xi_n = -\frac{1}{2}h + nh$ ,  $n = 0, 1, 2, \dots, N + 2$ , so that  $x_n$  is the center of the finite-difference block  $(\xi_n, \xi_{n+1})$ .

We define a uniform time grid by

$$t_j = jk \quad j = 0, 1, \dots$$

Consider the region in the  $xt$  plane defined by

$$\xi_n < x < \xi_{n+1} \quad t_j < t < t_{j+1}$$

If we integrate the differential equation conservation law Eq. (25) over this region, we get

$$\int_{t_j}^{t_{j+1}} \int_{\xi_n}^{\xi_{n+1}} (\rho_t + q_x) dx dt = \int_{\xi_n}^{\xi_{n+1}} \int_{t_j}^{t_{j+1}} \rho_t dt dx + \int_{t_j}^{t_{j+1}} \int_{\xi_n}^{\xi_{n+1}} q_x dx dt$$

$$\int_{\xi_n}^{\xi_{n+1}} [\rho(x, t_{j+1}) - \rho(x, t_j)] dx = \int_{t_j}^{t_{j+1}} [q(\xi_n, t) - q(\xi_{n+1}, t)] dt \tag{26}$$

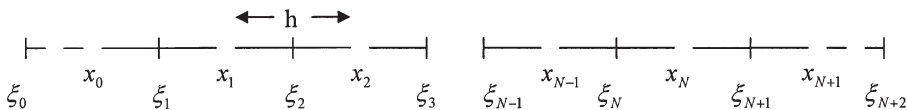


Figure 2. Block-centered finite-difference grid with uniform grid spacing.

We will use the midpoint quadrature rule to approximate the integral of the densities in Eq. (26):

$$\int_{\xi_n}^{\xi_{n+1}} [\rho(x, t_{j+1}) - \rho(x, t_j)] dx \cong [\rho(x_n, t_{j+1}) - \rho(x_n, t_j)]h \tag{27}$$

To approximate the integral of the fluxes in Eq. (26) in a manner consistent with the implicit, backward-in-time method, we choose the right endpoint quadrature rule to obtain

$$\int_{t_j}^{t_{j+1}} [q(\xi_n, t) - q(\xi_{n+1}, t)] dt = [q(\xi_n, t_{j+1}) - q(\xi_{n+1}, t_{j+1})]k \tag{28}$$

Here we use the trapezoidal rule to approximate Eq. (28):

$$[\rho(x_n, t_{j+1}) - \rho(x_n, t_j)]h = [q(\xi_n, t_{j+1}) - q(\xi_{n+1}, t_{j+1})]k \tag{29}$$

From  $q = -a(u)u_x$ , we have

$$u_x(x, t_{j+1}) = -\frac{q(x, t_{j+1})}{a[u(x, t_{j+1})]} \tag{30}$$

The integral of Eq. (30) from  $x_{n-1}$  to  $x_n$  gives

$$u_n^{j+1} - u_{n-1}^{j+1} = -\int_{x_{n-1}}^{x_n} \frac{q(x, t_{j+1})}{a[x, u(x, t_{j+1})]} dx \cong -q(\xi_n, t_{j+1}) \left\{ \frac{h(a_n^{j+1} + a_{n-1}^{j+1})}{2a_n^{j+1}a_{n-1}^{j+1}} \right\} \tag{31}$$

We introduce the harmonic averaged function as

$$f(a_m, a_n) = \frac{2a_m a_n}{a_m + a_n} \tag{32}$$

Also, to avoid a division by zero, we define  $f(0, 0) = 0$ .

Hence we have

$$\begin{aligned} q(\xi_n, t_{j+1}) &\cong -\frac{2a_n^{j+1}a_{n-1}^{j+1}}{(a_n^{j+1} + a_{n-1}^{j+1})} \frac{u_n^{j+1} - u_{n-1}^{j+1}}{h} \quad \text{or} \\ q(\xi_n, t_{j+1}) &\cong -f(a_n^{j+1}, a_{n-1}^{j+1})[u_n^{j+1} - u_{n-1}^{j+1}]/h \end{aligned} \tag{33}$$

For the problem under consideration, we have

$$p = U \quad q = -\frac{\mu(U_\eta) \partial U}{\mu_0 \partial \eta} \quad a(u) = \frac{\mu(U_\eta)}{\mu_0} \tag{34}$$

Introducing the notation

$$f_{n-1}^{j+1} = f(a_n^{j+1}, a_{n-1}^{j+1}) \quad f_{n+1}^{j+1} = f(a_n^{j+1}, a_{n+1}^{j+1}) \tag{35}$$

The nondimensionalized momentum equation can be expressed as

$$U_n^{j+1} - U_n^j = r \left[ f_{n-1}^{j+1} U_{n-1}^{j+1} - \left( f_{n-1}^{j+1} + f_{n+1}^{j+1} \right) U_n^{j+1} + f_{n+1}^{j+1} U_{n+1}^{j+1} \right] \tag{36}$$

where  $r = k/h^2$ .

The usual first approximation to the solution of the nonlinear difference equation is obtained by ‘‘lagging the nonlinearities.’’ That is, the coefficients in the difference equation are set at the  $t$  value, rather than the  $t + k$  value. If the nonlinearities in Eq. (36) are lagged, the result is the linear system

$$U_n^{j+1} - U_n^j = r \left[ f_{n-1}^j U_{n-1}^{j+1} - \left( f_{n-1}^j + f_{n+1}^j \right) U_n^{j+1} + f_{n+1}^j U_{n+1}^{j+1} \right] \tag{37}$$

Using a procedure similar to the Crank-Nicholson method, we get the finite-difference equation as

$$\begin{aligned} -\frac{r}{2} f_{n-1}^j U_{n-1}^{j+1} + \left[ 1 + \frac{r}{2} \left( f_{n-1}^j + f_{n+1}^j \right) \right] U_n^{j+1} \\ - \frac{r}{2} f_{n+1}^j U_{n+1}^{j+1} = U_n^j (1 - r) + \frac{r}{2} \left( U_{n-1}^j + U_{n+1}^j \right) \end{aligned} \tag{38}$$

Since we have already obtained the velocity gradient, namely,  $(U_\eta)^j_n$ , in the process of solving the momentum equation, we introduce the Crank-Nicholson method to discretize the energy equation given by Eq. (21).

Similarly, the finite-difference form of the energy equation can then be obtained as

$$\begin{aligned} \theta_n^{j+1} - \theta_n^j = \frac{1}{\text{Pr}} \frac{k}{2h^2} \left( \theta_{n-1}^{j+1} - 2\theta_n^{j+1} + \theta_{n+1}^{j+1} + \theta_{n-1}^j - 2\theta_n^j + \theta_{n+1}^j \right) \\ + \text{Ek} \frac{\mu_n^j}{\mu_0} \left[ (U_\eta)^j_n \right]^2 \end{aligned} \tag{39}$$

or

$$\begin{aligned} -\frac{1}{\text{Pr}} \frac{r}{2} \theta_{n-1}^{j+1} + \left( 1 + \frac{r}{\text{Pr}} \right) \theta_n^{j+1} - \frac{1}{\text{Pr}} \frac{r}{2} \theta_{n+1}^{j+1} = \left( 1 - \frac{r}{\text{Pr}} \right) \theta_n^j \\ + \frac{1}{\text{Pr}} \frac{r}{2} \left( \theta_{n-1}^j + \theta_{n+1}^j \right) + \text{Ek} \frac{\mu_n^j}{\mu_0} \left[ (U_\eta)^j_n \right]^2 \end{aligned} \tag{40}$$

where  $r = k/h^2$ .

For a Newtonian fluid, an analytical solution for the temperature distribution is established utilizing the classical analytical velocity distribution and using the following transformation:

$$s = \sqrt{\text{Pr}} \eta \tag{41}$$

Equation (21) can then be written as

$$\frac{\partial \theta}{\partial \tau} = \frac{\partial^2 \theta}{\partial s^2} + \text{Pr Ek} \left( \frac{\partial U}{\partial s} \right)^2 \tag{42}$$

where  $\partial U/\partial s$  can be obtained from the velocity solution of Erdogan [2] or Khaled and Vafai [3] for the no-slip case.

The initial and boundary conditions will be

$$\theta(0, \tau) = 1 \quad \theta_s(\infty, \tau) = 0 \quad \theta(s, 0) = 0 \tag{43}$$

Letting  $g(s, \tau) = \text{Pr Ek}(\partial U/\partial s)^2$ , the solution of Eq. (42) can be formed as [18]

$$\begin{aligned} \theta(\eta, \tau) = & \frac{s}{2\sqrt{\pi}} \int_{t=0}^{\tau} \frac{1}{(\tau-t)^{3/2}} e^{-[s^2/4(\tau-t)]} dt + \frac{1}{2\sqrt{\pi}} \int_{t=0}^{\tau} \frac{1}{\sqrt{\tau-t}} \int_{x=0}^{\infty} g(x, t) \\ & \times \{e^{-[(s-x)^2/4(\tau-t)]} - e^{-[(s+x)^2/4(\tau-t)]}\} dx dt \end{aligned} \tag{44}$$

### 6. NUMERICAL SIMULATION AND DISCUSSION

Numerical results for the nondimensional velocity  $U(\eta, \tau)$  have been obtained for each boundary condition and for various viscosity models. It has been found that the non-Newtonian flows also achieve a steady periodic state. It should be noted that when the power index  $n = 1$  for the power-law model or when the generalized shear rate  $\dot{\gamma} \rightarrow 0$  for other models, the numerical results obtained here agree well with the exact solution of Khaled and Vafai [3] for the Newtonian flow with no-slip condition.

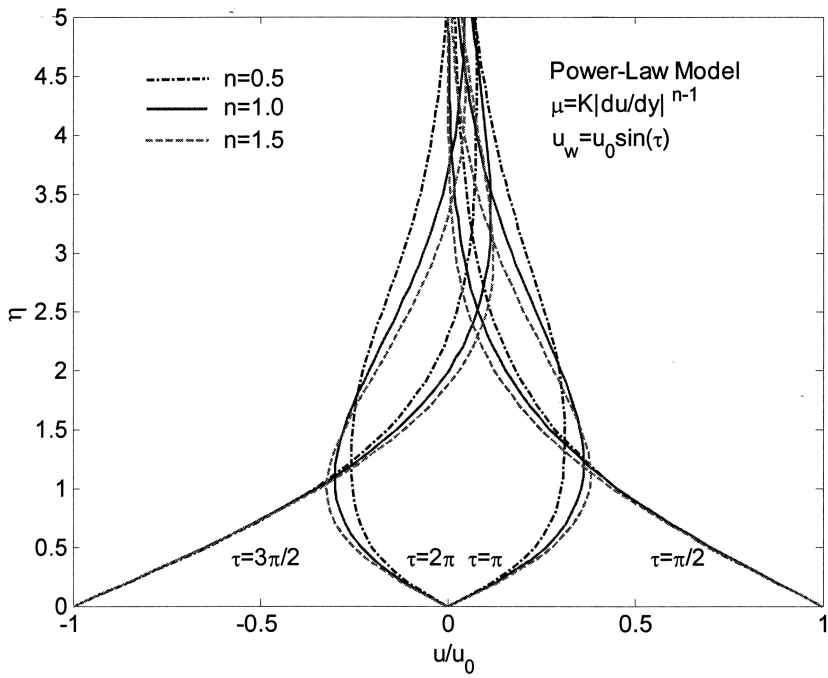
In Figure 3a, the velocity profile is presented when the boundary condition is  $u_w = U_0 \sin wt$  for various values of power index  $n$  for the power-law model. The value at  $n = 1$  refers to a Newtonian fluid. The following correlation is obtained for calculating the velocity distribution with the power-index range from  $n = 0.6$  to  $n = 1.6$ :

$$\begin{aligned} U = & U_N + 2.4 \times (-0.18\eta^3 + 0.55\eta^{2.5} + \eta^{0.9}) \times \exp(-2.35\eta^{0.57}n^{0.16}) \\ & \times \cos(\tau - 2.35\eta^{0.57}n^{0.16}) \times [(n-1) - 1.27(n-1)^2 + 0.88(n-1)^3] \\ & \times \cos(-0.08\eta^{1.28}n^{1.8} + 1.5) \end{aligned} \tag{45}$$

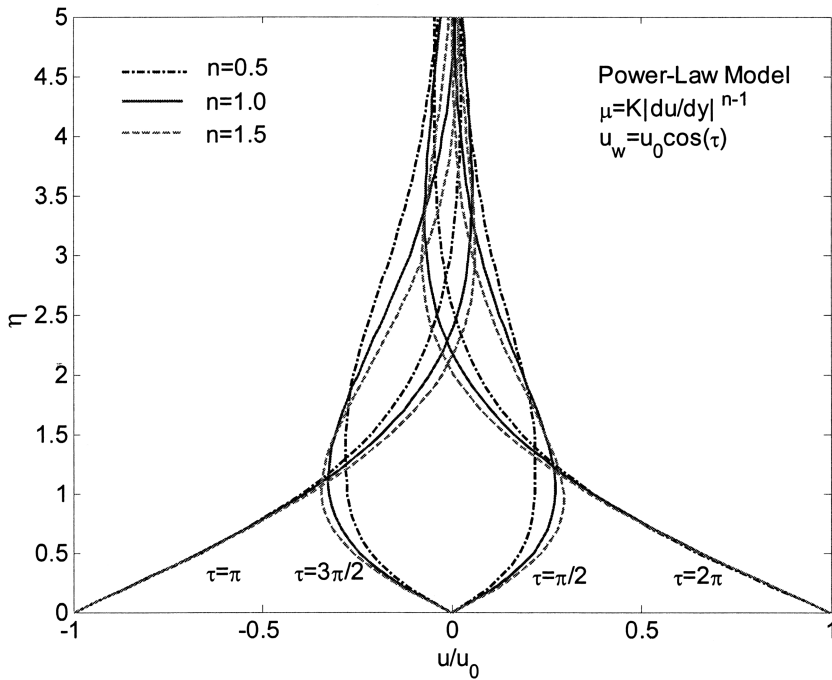
where  $U_N$  is the classical analytical velocity distribution for a Newtonian fluid.

Figure 4a illustrates the effects of the power index  $n$  on the time required to reach steady periodic flow under the boundary condition utilized in Figure 3a. The time required to reach steady periodic flow was evaluated based on the dimensionless time for the average dimensionless transient velocity reaching a value of 0.05. The results show that power index strongly affects the time required for reaching steady periodic flow conditions. A power-index value of  $n \simeq 0.65$  is found to correspond to the maximum time required to reach steady periodic flow conditions. Dimensionless parameter  $\kappa = (K/\mu_0)U_0^{n-1}(\omega/\nu_0)^{(n-1)/2}$  in Eq. (19) corresponds to 1 in this case. For the power-index range from  $n = 0.2$  to  $n = 1.6$ , the following correlation is obtained for calculating time required for reaching steady periodic flow conditions:

$$\tau = \frac{0.2797 + 0.9229n + 1.9433n^2 - 3.5901n^3}{1 - 3.311n + 6.0743n^2 - 4.1052n^3 + 0.1274n^4} \tag{46}$$

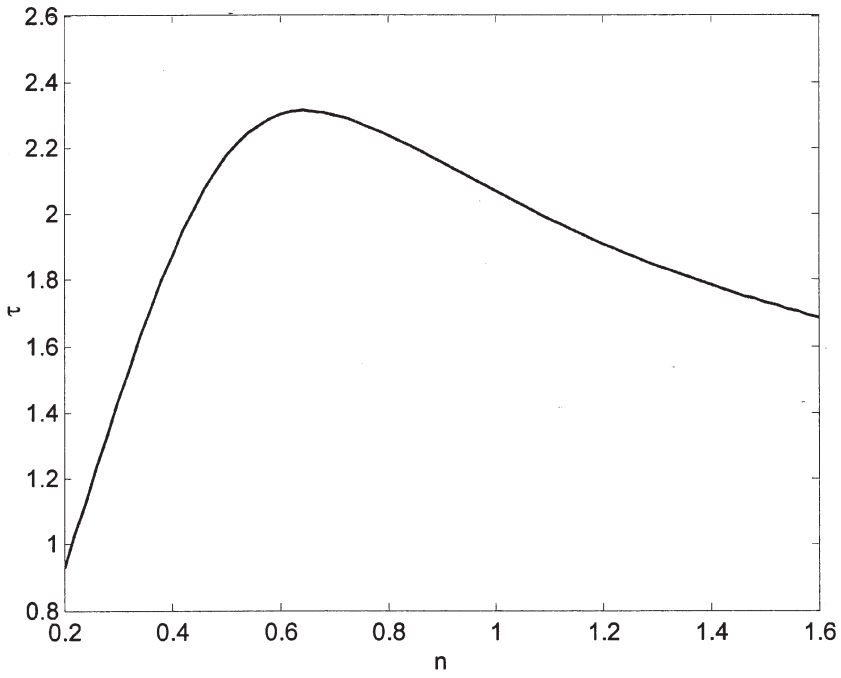


(a)  $U(0, \tau) = \sin \tau$

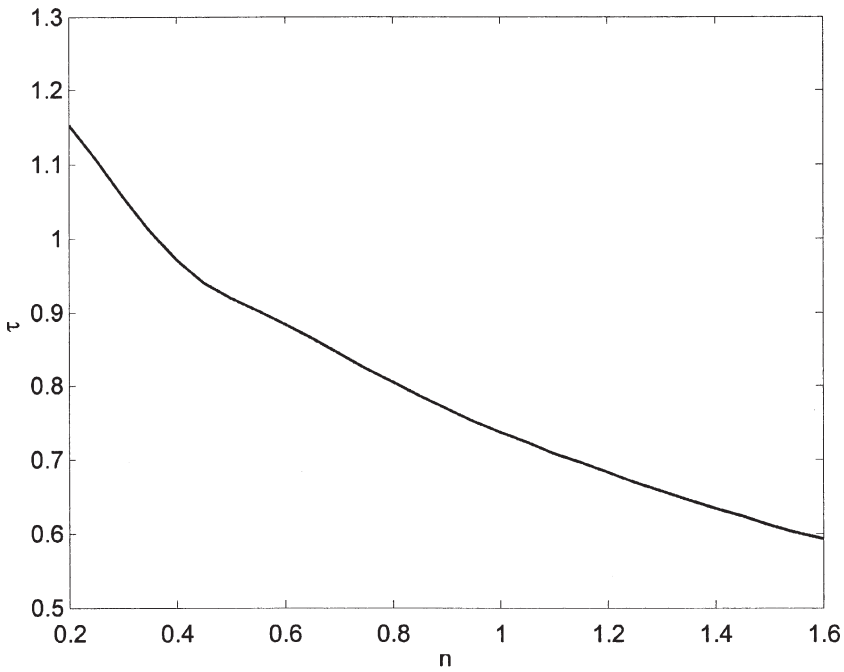


(b)  $U(0, \tau) = \cos \tau$

Figure 3. Effects of power index  $n$  on the velocity profile for the power-law model.



(a)  $U(0, \tau) = \sin \tau$



(b)  $U(0, \tau) = \cos \tau$

Figure 4. Effects of power index  $n$  on the time needed to reach steady periodic flow.

In Figure 3*b*, the velocity profile is presented when the boundary condition is  $u_w = U_0 \cos \omega t$  for various values of the power index  $n$  in the power-law model. Figure 4*b* illustrates the effects of the power index  $n$  on the time required to reach steady periodic flow under the cosine boundary condition. Comparing Figures 3*a* and 3*b*, we can see that the effect of the boundary condition is more pronounced than the effect of the power index. For the power-index range from  $n = 0.2$  to  $n = 1.6$ , the following correlation is obtained for calculating the time required for reaching steady periodic flow conditions when the cosine boundary condition is specified at the wall:

$$\tau = \frac{1.5984 - 8.1767n + 11.9971n^2 - 2.4893n^3 - 1.8727n^4}{1 - 2.8162n - 5.1123n^2 + 20.4959n^3 - 12.9093n^4 + 1.0513n^5} \quad (47)$$

Our results illustrate that an increase in the power index delays the oscillatory boundary condition effects shown in Figures 3*a* and 3*b*.

Figures 5–7 illustrate the effects of dimensionless parameter  $\kappa$  and Ek number on the velocity and temperature distribution due to cosine oscillations. From Figure 5 we see that the effect of dimensionless parameter  $\kappa$  is to increase the velocity boundary-layer thickness and the temperature boundary-layer thickness. Eckert number has a similar effect only on the temperature boundary-layer thickness. From Figure 5 it is evident that increasing the dimensionless parameter  $\kappa$  increases the thickness of the velocity boundary layer, while it has just a slight effect on the thickness of the thermal boundary layer. However, the effect of Eckert number on the temperature distribution is more pronounced than the effect of dimensionless parameter  $\kappa$ , as shown in Figure 6. Due to the large velocity gradient near the wall, the dissipation term in Eq. (9) is quite significant.

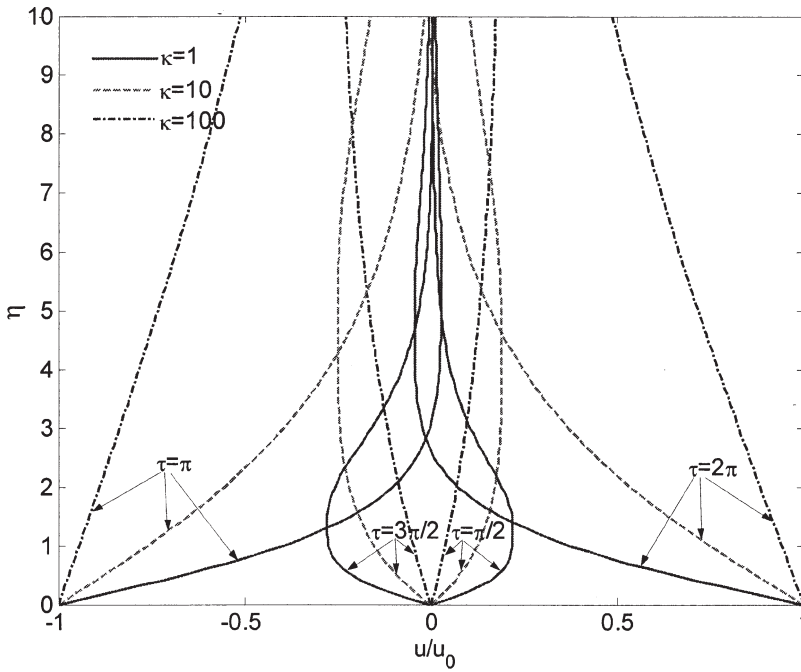
From Figure 7, it can be seen that increasing the Prandtl number decreases the thickness of the thermal boundary layer due to the dissipation term. This is consistent with the thermal boundary-layer thickness obtained from Stokes' second problem. The combined effects of  $\kappa$  and Ek on the velocity and temperature profiles are shown in Figure 8. The effects of power index  $n$  and viscosity ratio  $\mu_\infty/\mu_0$  on other models are shown in Figures 9–13.

To study the non-Newtonian behavior of blood under unsteady condition, we define the reference shear rate  $\dot{\gamma}_0$  as

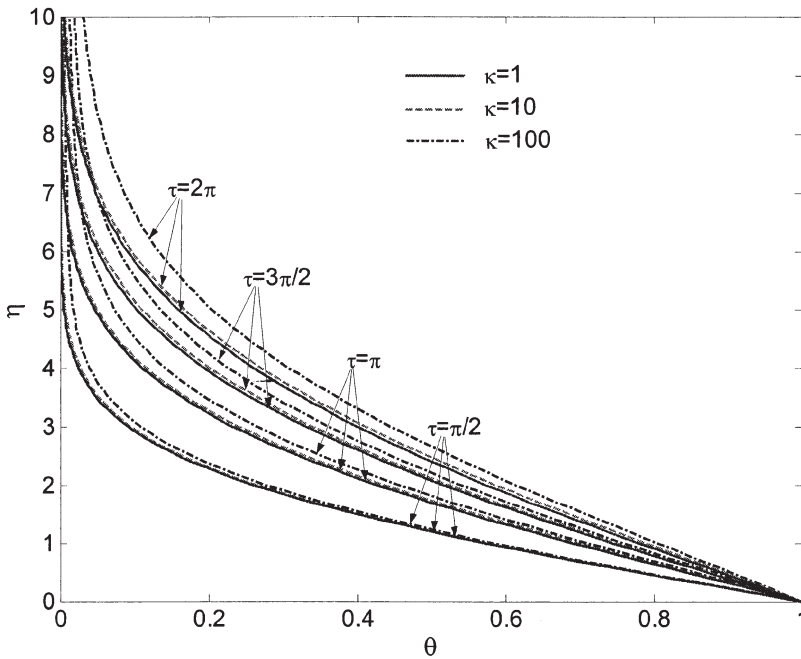
$$\dot{\gamma}_0 = U_0 \left( \frac{\omega}{\nu_0} \right)^{1/2} \quad (48)$$

which represents the magnitude of the wall shear rate as a combination effect of the reference velocity  $U_0$ , representative viscosity of the Newtonian fluid  $\nu_0$ , and frequency of the vibration  $\omega$ .

From Figure 14, one can see that the velocity pattern is consistent across all models at both high and low shear rates, while the magnitude of velocity is greater at high shear rate. Figure 15 represents the effect of the reference shear rate  $\dot{\gamma}_0$  on the wall shear stress for different blood models. It can be seen that the magnitude of wall shear stress is affected significantly by  $\dot{\gamma}_0$ . While the pattern of wall shear stress is consistent across all the models, the magnitude was influenced by the model utilized.

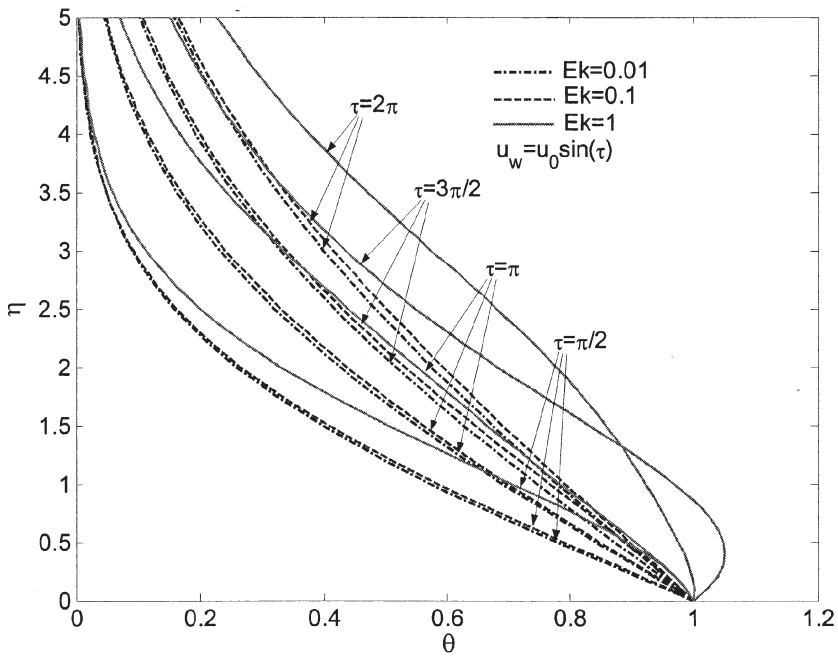


(a) Velocity profile

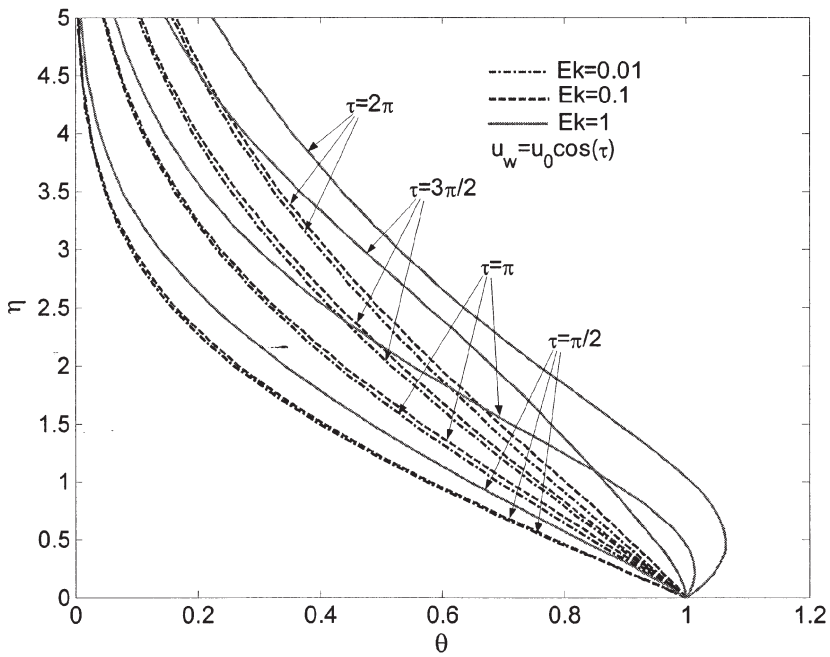


(b) Temperature profile

Figure 5. Effects of parameter  $\kappa$  on the velocity and temperature profiles for the power-law model.

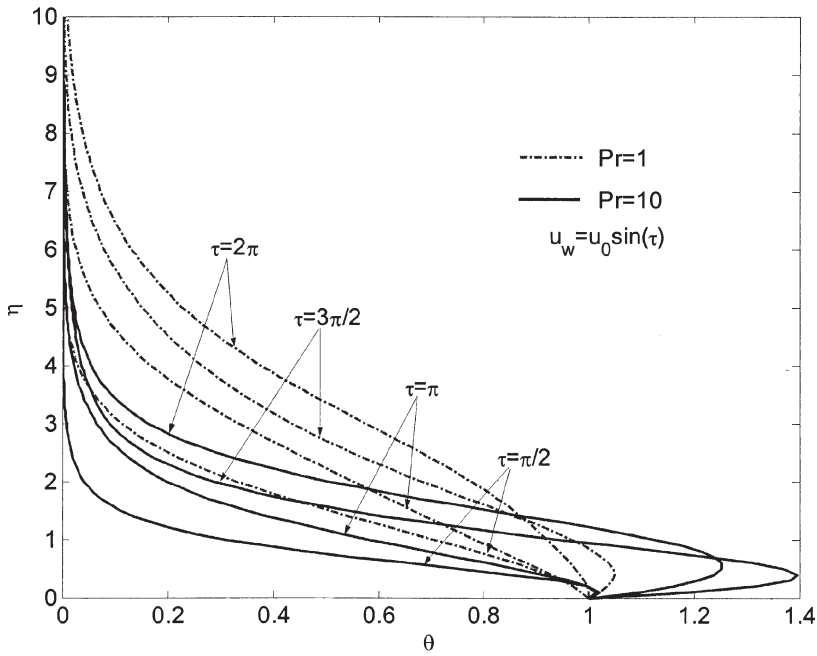


(a)  $U(0, \tau) = \sin \tau$

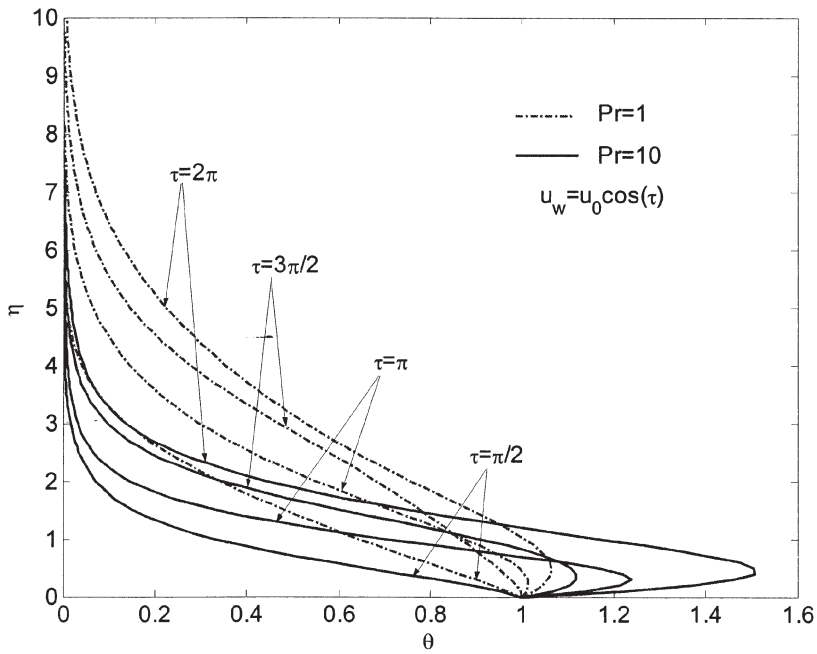


(b)  $U(0, \tau) = \cos \tau$

Figure 6. Effects of parameter Ek on the temperature profile for the power-law model.

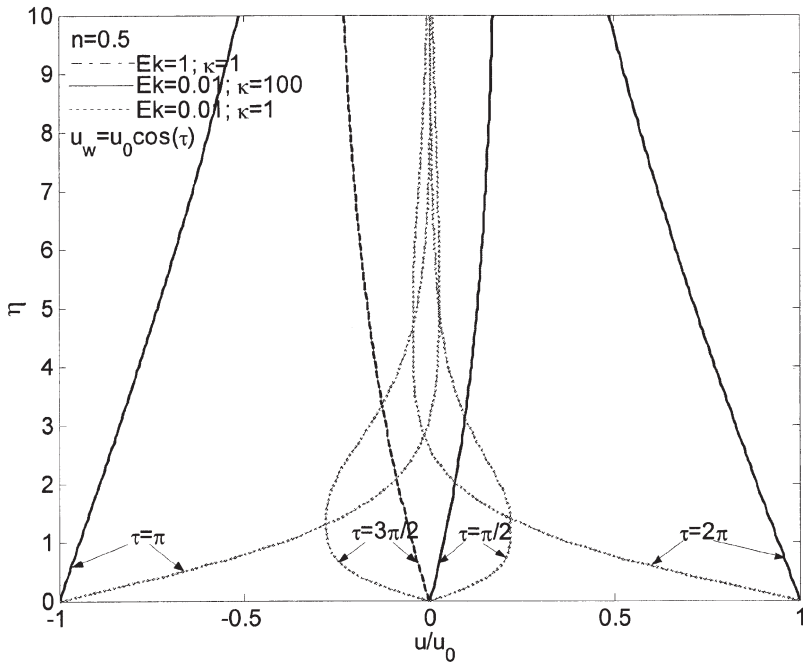


(a)  $U(0, \tau) = \sin \tau$

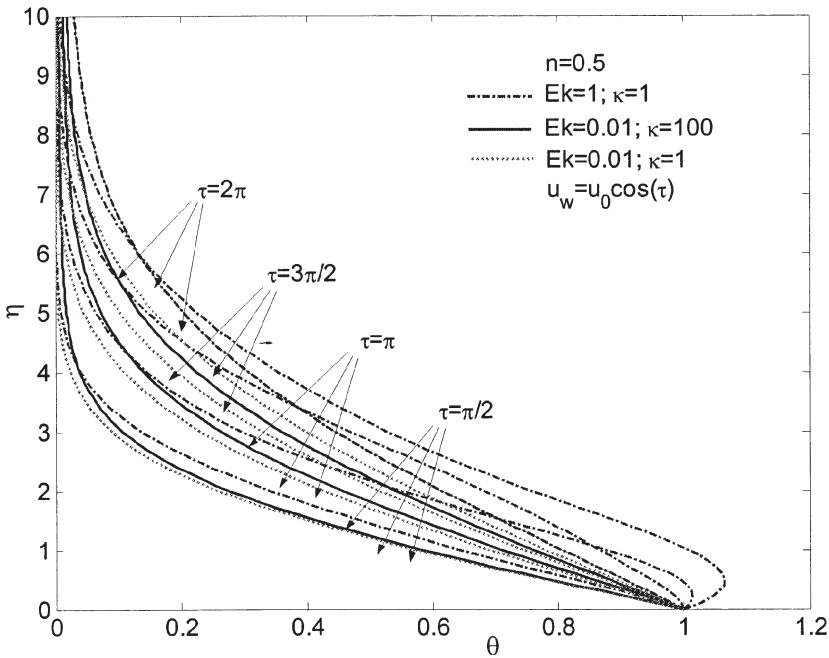


(b)  $U(0, \tau) = \cos \tau$

Figure 7. Effects of parameter Pr on the temperature profile for the power-law model.

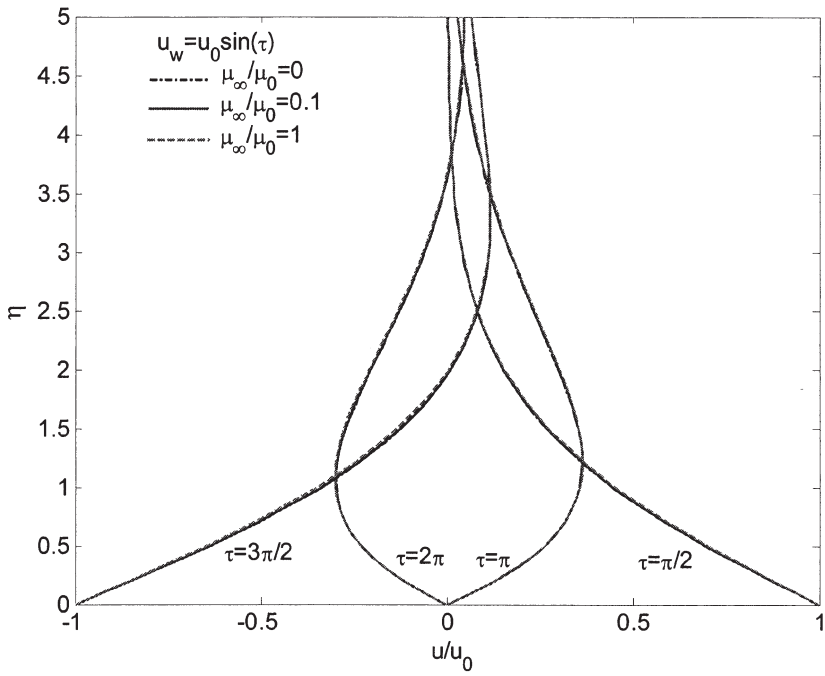


(a) Velocity profile

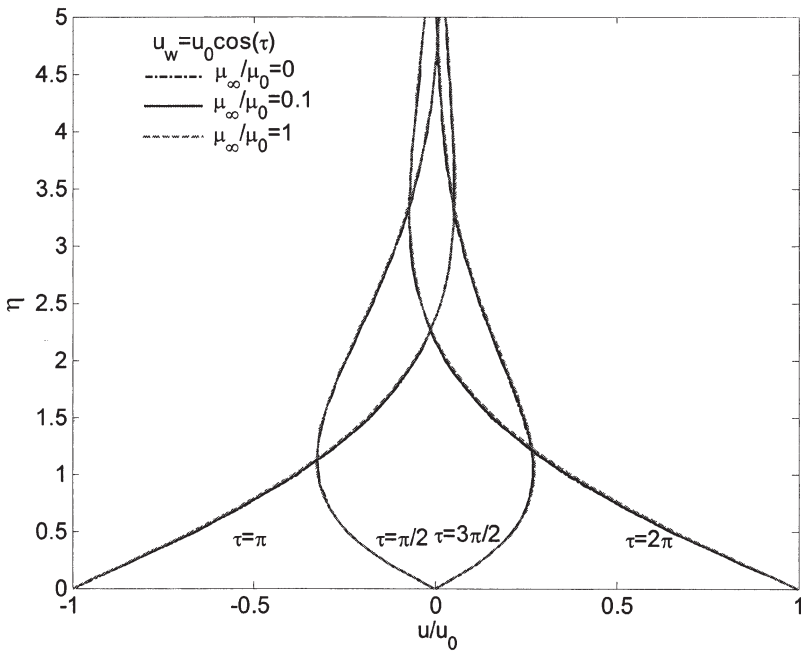


(b) Temperature profile

Figure 8. Combined effects of  $\kappa$  and  $Ek$  on the velocity and temperature profiles.

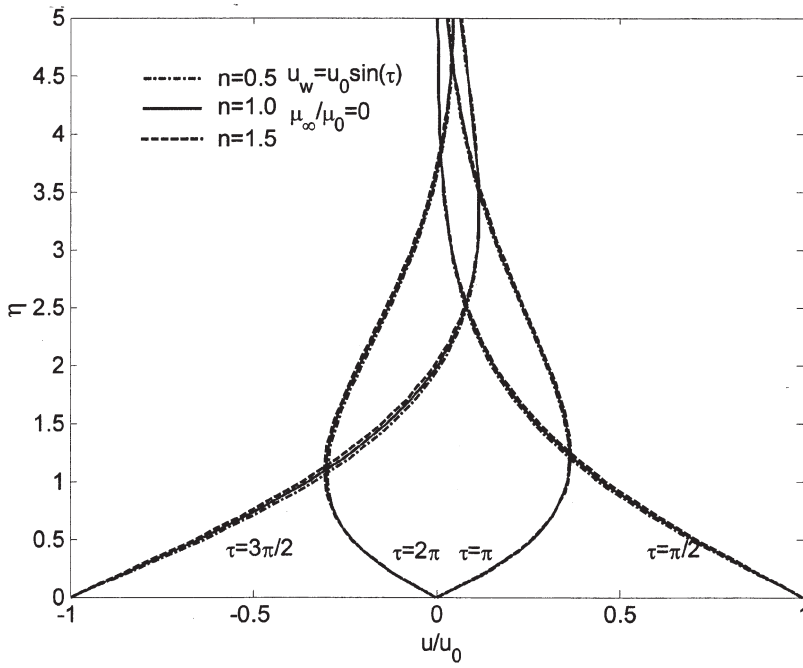


(a)  $U(0, \tau) = \sin \tau$

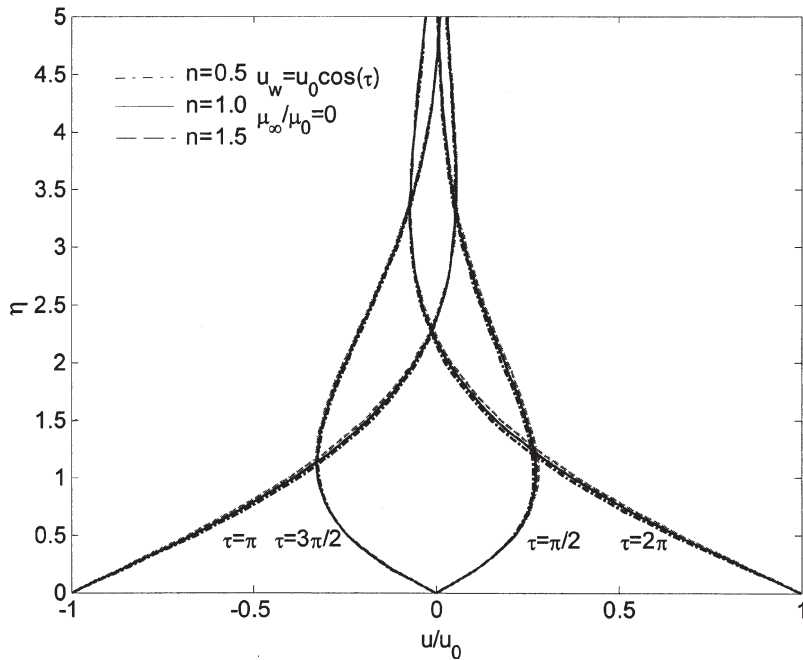


(b)  $U(0, \tau) = \cos \tau$

Figure 9. Effects of viscosity ratio  $\mu_\infty/\mu_0$  on the velocity profile for the Powell-Eyring model.

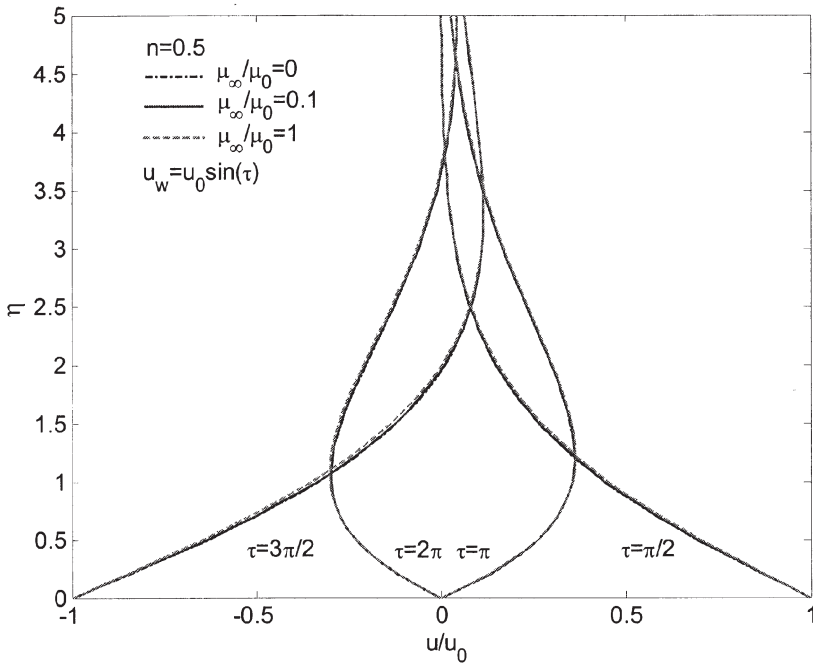


(a)  $U(0, \tau) = \sin \tau$

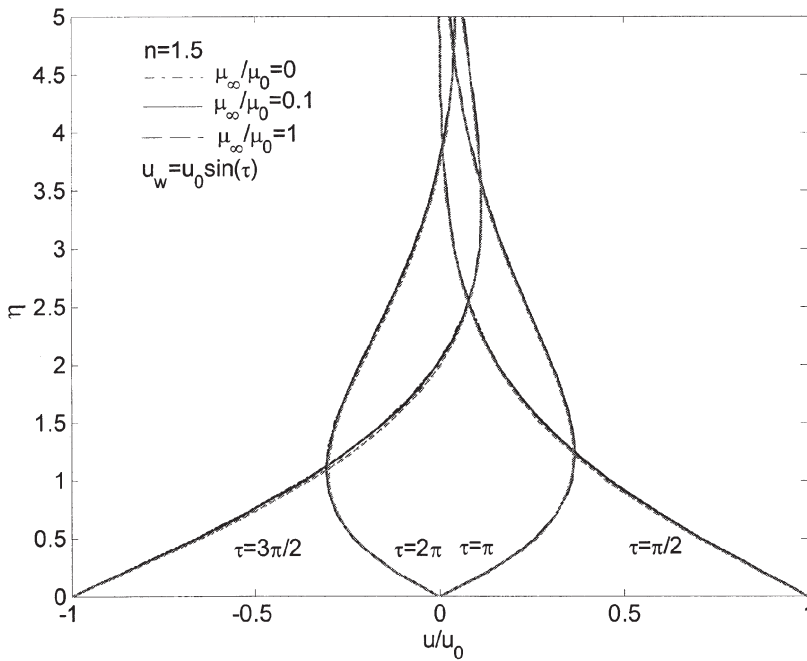


(b)  $U(0, \tau) = \cos \tau$

Figure 10. Effects of power index  $n$  on the velocity profile for the Carreau model.

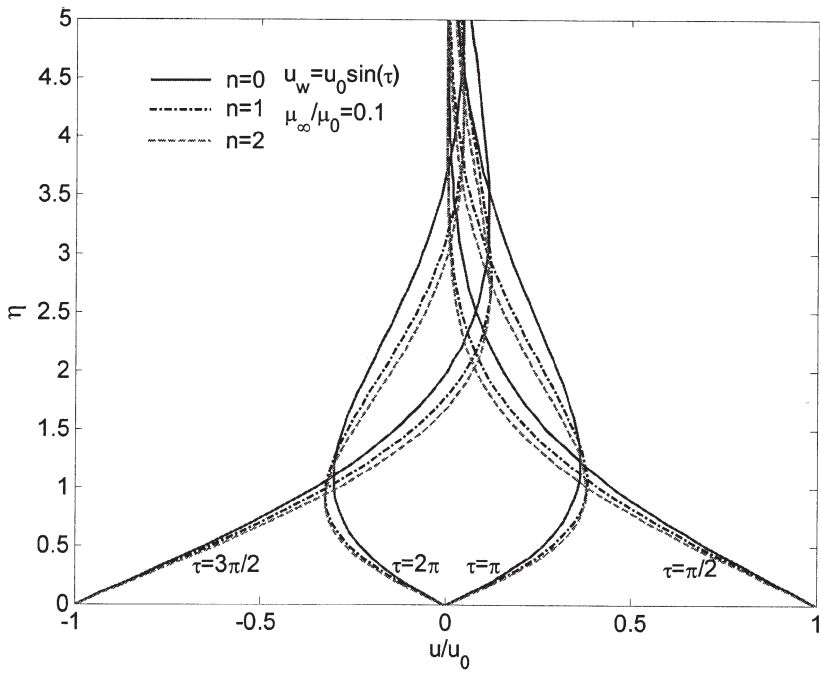


(a)  $n = 0.5$

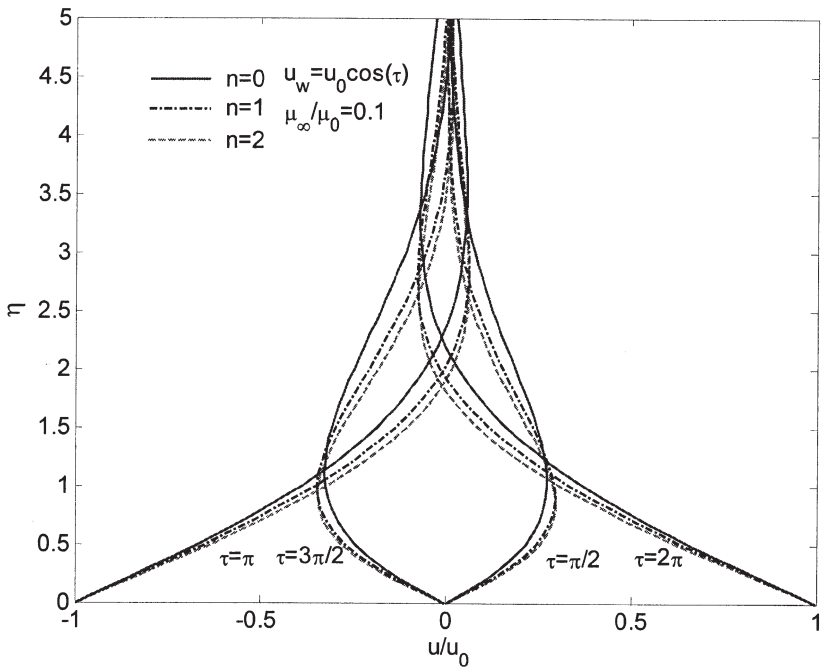


(b)  $n = 1.5$

Figure 11. Effects of viscosity ratio  $\mu_\infty/\mu_0$  on the velocity profile for the Carreau model.

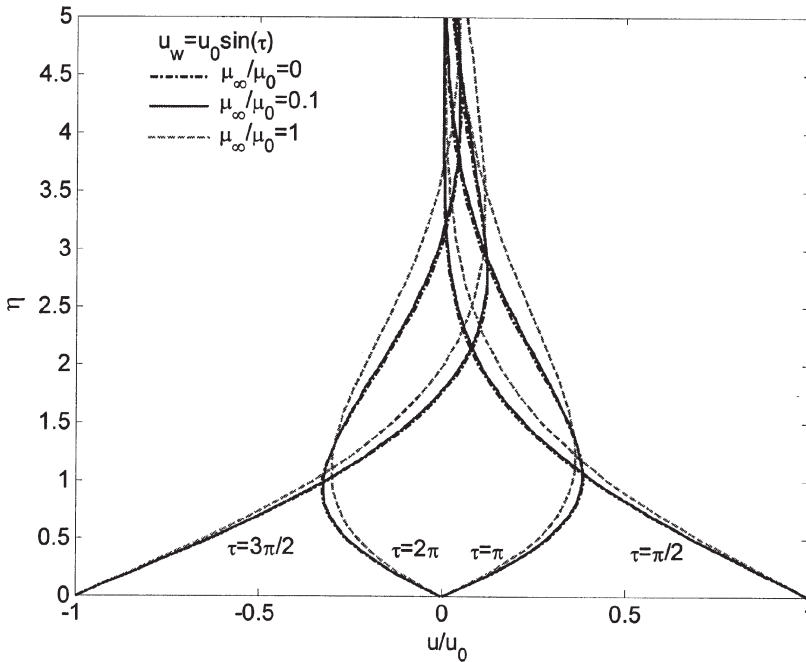


(a)  $U(0, \tau) = \sin \tau$

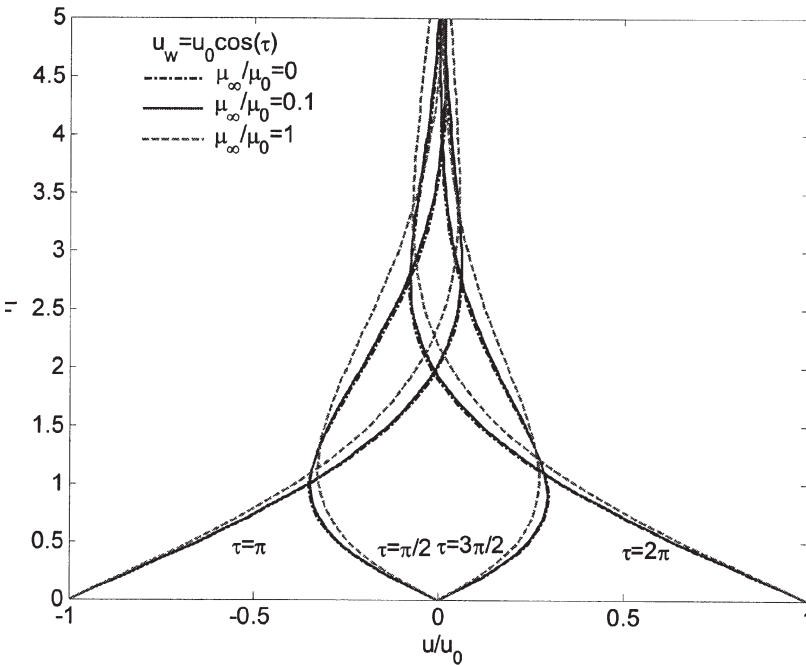


(b)  $U(0, \tau) = \cos \tau$

Figure 12. Effects of power index  $n$  on the velocity profile for the hyperbolic tangent model.

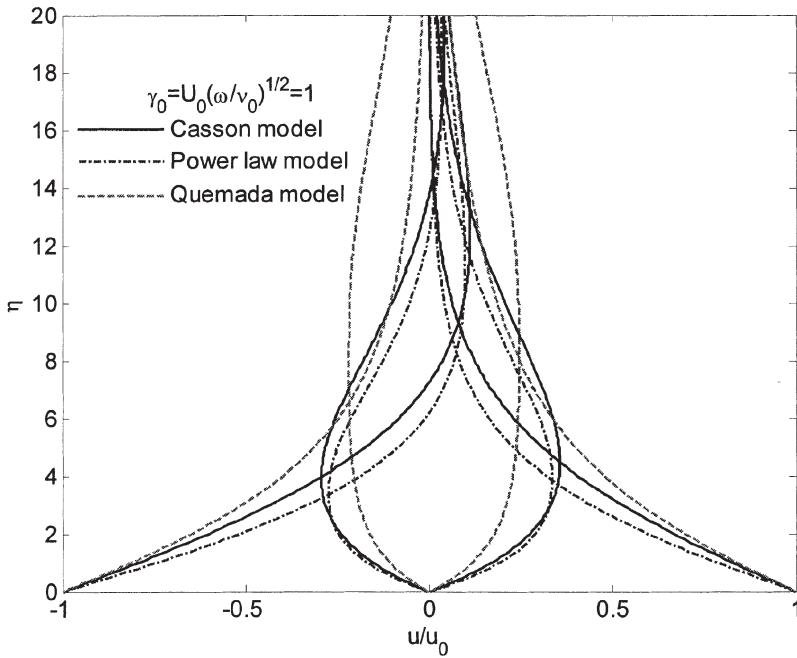


(a)  $U(0, \tau) = \sin \tau$

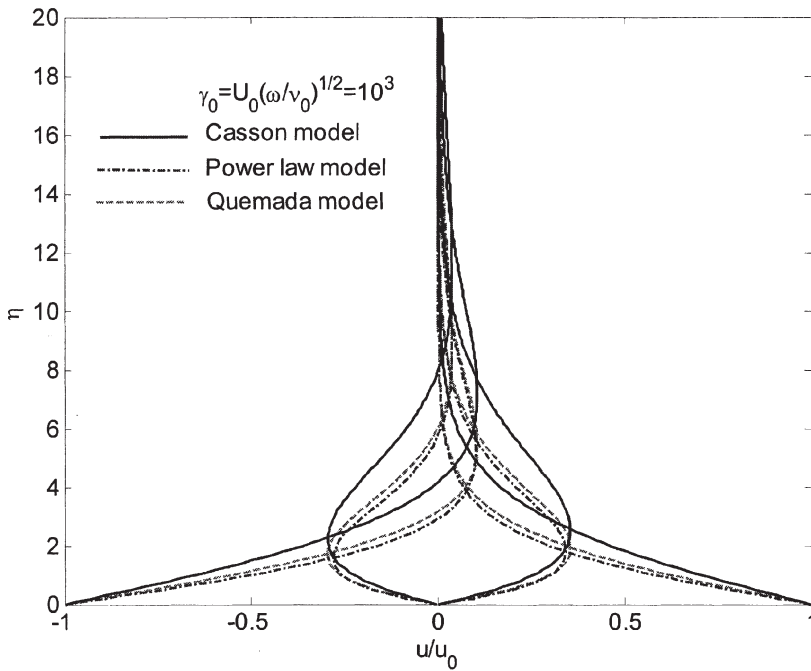


(b)  $U(0, \tau) = \cos \tau$

Figure 13. Effects of viscosity ratio  $\mu_\infty/\mu_0$  on the velocity profile for the hyperbolic tangent model.

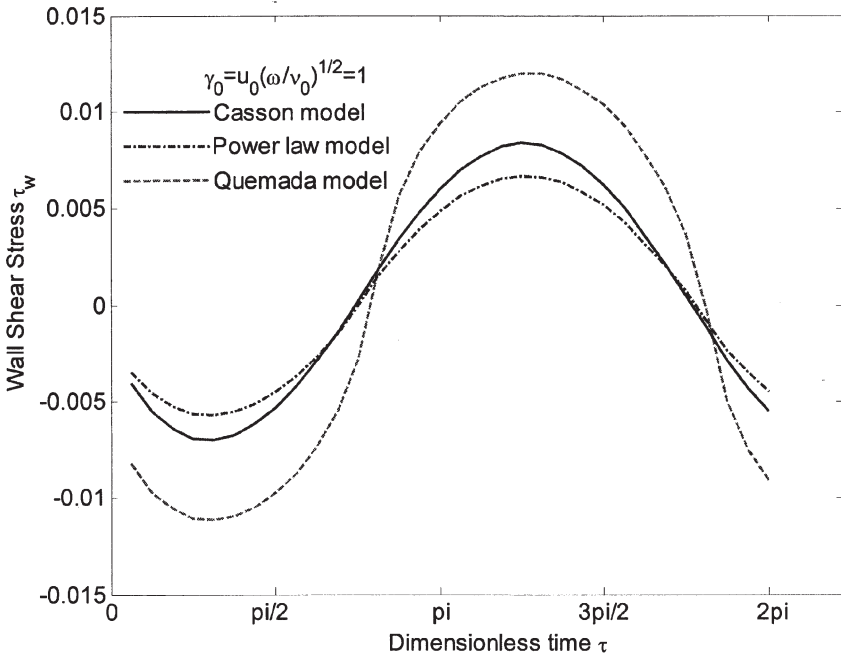


(a)  $\gamma_0 = 1, U(0, \tau) = \sin \tau$

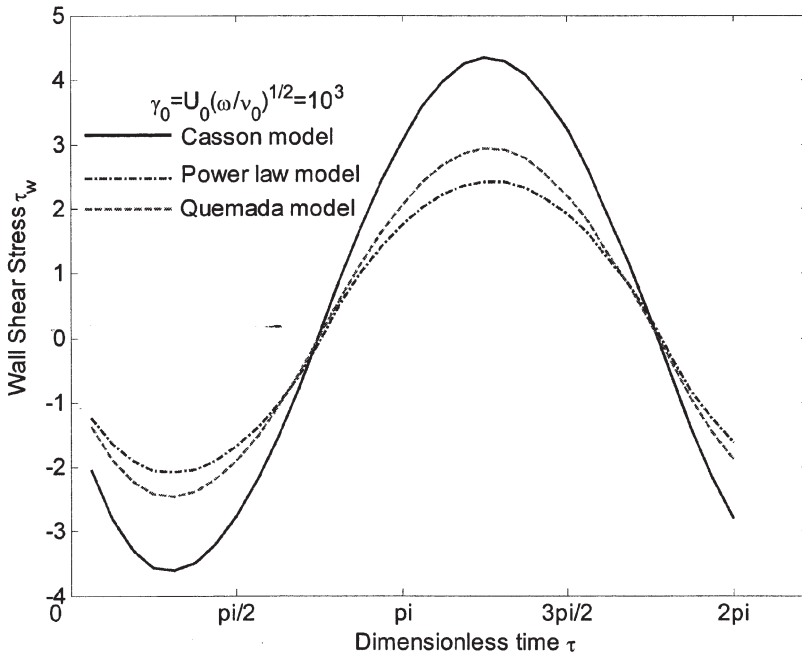


(b)  $\gamma_0 = 1000, U(0, \tau) = \sin \tau$

Figure 14. Effects of reference shear rate  $\gamma_0$  on the velocity profile for different blood models.



(a)  $\gamma_0 = 1, U(0, \tau) = \sin \tau$



(b)  $\gamma_0 = 1000, U(0, \tau) = \sin \tau$

Figure 15. Effects of reference shear rate  $\gamma_0$  on the wall shear stress for different blood models.

## 7. CONCLUSIONS

In this article, effects of non-Newtonian flow on Stokes' second problem were investigated. The wall was subjected to both sine and cosine oscillations. The temperature variation near the wall was also investigated. Several pertinent viscosity models for non-Newtonian fluids were introduced. The governing equations were nondimensionalized and solved by introducing a mass-balance procedure. The velocity and temperature profiles for various viscosity models were obtained and the results were compared to those obtained for the Newtonian fluids. For the power-law model, the time required to reach steady periodic flow for various power-law indices was established. Correlations for the velocity distribution and the time required to reach steady periodic flow conditions were developed. The effects of the dimensionless parameters, such as power index  $n$  and  $Ek$ , on the flow were analyzed, and an analytical solution for the temperature distribution for the Newtonian case was obtained. It was also found that in the case of unsteady Stokes flow, while the flow patterns are consistent across all models, the magnitude was affected significantly by the reference shear rate and the model utilized.

## REFERENCES

1. H. Schlichting, *Boundary Layer Theory*, 6th ed., McGraw-Hill, New York, 1968.
2. M. E. Erdogan, A Note on Unsteady Flow of a Viscous Fluid due to an Oscillating Plane Wall, *Int. J. Non-Linear Mech.*, vol. 35, pp. 1–6, 2000.
3. A.-R. A. Khaled and K. Vafai, The Effect of the Slip Condition on Stokes and Couette Flows due to an Oscillating Wall: Exact Solutions, *Int. J. Non-Linear Mech.*, vol. 39, pp. 795–809, 2004.
4. B. M. Johnston, P. R. Johnston, S. Corney, and D. Kilpatrick, Non-Newtonian Blood Flow in Human Right Coronary Arteries: Steady State Simulations, *J. Biomech.*, vol. 37, pp. 709–720, 2004.
5. E. L. Allgower and K. Georg, *Computational Solution of Nonlinear Systems of Equations*, American Mathematical Society, Providence, RI, 1990.
6. J. F. Agassant, P. Avenas, J. Ph. Sergent, and P. J. Carreau, *Polymer Processing: Principles and Modeling*, Hanser, New York, 1991.
7. I. Pop and D. B. Ingham, *Convective Heat Transfer: Mathematical and Computational Modelling of Viscous Fluids and Porous Media*, Pergamon, Amsterdam, New York, 2001.
8. G. Astarita and G. Marrucci, *Principles of Non-Newtonian Fluid Mechanics*, McGraw-Hill, New York, 1974.
9. A. H. P. Skelland, *Non-Newtonian Flow and Heat Transfer*, Wiley, New York, 1967.
10. P. Neofytou and D. Drikakis, Non-Newtonian Flow Instability in a Channel with a Sudden Expansion, *J. Non-Newtonian Fluid Mech.*, vol. 111, pp. 127–150, 2003.
11. N. Casson, A Flow Equation for the Pigment Oil Suspensions of the Printing Ink Type, in *Rheology of Disperse Systems*, pp. 84–102, Pergamon, New York, 1959.
12. S. Charm and G. Kurland, Viscometry of Human Blood for Shear Rates of 0–100,000  $s^{-1}$ . *Nature (Lond.)*, vol. 206, pp. 617–618, 1965.
13. T. C. Papanastasiou, Flows of Materials with Yield, *J. Rheol.*, vol. 31, pp. 385–404, 1987.
14. T. V. Pham and E. Mitsoulis, Entry and Exit Flows of Casson Fluids, *Can. J. Chem. Eng.*, vol. 72, p. 1080, 1994.

15. D. Quemada, Rheology of Concentrated Disperse Systems. III. General Features of the Proposed Non-Newtonian Model. Comparison with Experimental Data, *Rheol. Acta*, vol. 17, p. 643, 1977.
16. S. E. Charm, W. McComis, and G. Kurland, Rheology and Structure of Blood Suspension, *J. Appl. Physiol.*, vol. 19, p. 127, 1964.
17. F. J. Walburn and D. J. Schneck, A Constitutive Equation for Whole Human Blood, *Biorheology*, vol. 13, p. 201, 1976.
18. M. D. Mikhailov and M. N. Özişik, *Unified Analysis and Solutions of Heat and Mass Diffusion*, Wiley, New York, 1984.